The quench action approach for integrable models: A Monte Carlo implementation

Authors

Abstract.
fdasfa

1. Introduction

We show that it is possible to numerically simulate the Quench Action approach combining Monte Carlo methods and Bethe ansatz techniques.
We focus on the situation in which the pre-quench initial state is the Neel state or the Majumdar-Ghosh state.
We investigate the importance of the zero-momentum strings in the Quench Action.
Without zero-momentum strings the overlap saturation rules are not valid, i.e., in finite size systems the vast majority of the eigenstates contain zero momentum strings.
The details on the eigenstates counting depend on the pre-quench initial state.
However, we show that one can restrict to the set of non-zero momentum strings. The fact that one neglects zero-momentum strings gives rise only to scaling corrections.
We also investigate the validity of the Bethe-Takahashi approximation for the calculation of the overlap.
In the thermodynamic limit it is natural to assume that the steady-state expectation values are obtained using the so-called diagonal ensemble, which is defined as

$$\langle \mathcal{O} \rangle = \sum_{\alpha} |\langle \Psi_0 | \alpha \rangle|^2 \langle \alpha | \mathcal{O} | \alpha \rangle. \tag{1}$$

It is useful to rewrite (1) as

$$\langle \mathcal{O} \rangle = \sum_{\alpha} \rho^{DE}(\alpha) \langle \alpha | \mathcal{O} | \alpha \rangle, \quad \text{with} \quad \rho^{DE}(\alpha) = \exp(-2\Re \mathcal{E}(\alpha)). \tag{2}$$

Here $\rho^{DE}(\alpha)$ is a diagonal ensemble density matrix, and $\mathcal{E}(\alpha) \equiv -\log\langle \alpha | \Psi_0 \rangle$, with $\Re$ denoting the real part.

2. Bethe ansatz solution of the Heisenberg (XXX) spin chain

Here we review some Bethe ansatz results for the spin-$\frac{1}{2}$ Heisenberg (XXX) chain. Specifically, in section 2.1 we introduce the model. Its eigenstates (Bethe states) and the Bethe equations are discussed in section 2.2. Section 2.3 focuses on the string hypothesis and the so-called Bethe-Gaudin-Takahashi (BGT) equations. The form of the BGT equations in the thermodynamic limit is discussed in section 2.4. Finally, in section 2.5 we provide some exact formulas for the local conserved charges of the model.

2.1. The spin-$\frac{1}{2}$ Heisenberg chain

The spin-$\frac{1}{2}$ isotropic Heisenberg chain (XXX chain) with L sites is defined by the Hamiltonian

$$\mathcal{H} \equiv J \sum_{i=1}^{L} \left[\frac{1}{2}(S_i^+ S_{i+1}^- + S_i^- S_{i+1}^+) + S_i^z S_{i+1}^z - \frac{1}{4} \right], \tag{3}$$

where $S_i^{\pm} \equiv (\sigma_i^x \pm i\sigma_i^y)/2$ are spin operators acting on the site i, $S_i^z \equiv \sigma_i^z/2$, and $\sigma_i^{x,y,z}$ the Pauli matrices. We fix $J = 1$ and use periodic boundary conditions, identifying sites

$L+1$ and 1. The total magnetization $S^z_T \equiv \sum_i S^z_i = L/2 - M$, with M number of down spins (particles), commutes with (3), and it is here used to label its eigenstates.

2.2. Bethe equations and wavefunctions

In the Bethe ansatz framework [29, 17] the generic eigenstate of (3) (Bethe state) in the sector with M particles can be written as

$$|\Psi_M\rangle = \sum_{1\leq x_1<x_2<\ldots<x_M\leq L} A_M(x_1, x_2, \ldots, x_M)|x_1, x_2, \ldots, x_M\rangle, \tag{4}$$

where the sum is over the positions $\{x_i\}_{i=1}^M$ of the particles, and $A_M(x_1, x_2, \ldots, x_M)$ is the eigenstate amplitude corresponding to the particles being at positions $x_1, x_2, \ldots, x_M$. Here $A_M(x_1, x_2, \ldots, x_M)$ is given as

$$A_M(x_1, x_2, \ldots, x_M) \equiv \sum_{\sigma\in S_M} \exp\Big[i\sum_{j=1}^M k_{\sigma_j}x_j + i\sum_{i<j}\theta_{\sigma_i,\sigma_j}\Big], \tag{5}$$

where the outermost summation is over the permutations S_M of the so-called quasi-momenta $\{k_\alpha\}_{\alpha=1}^M$. The two-particle scattering phases $\theta_{\alpha,\beta}$ are defined as

$$\theta_{\alpha,\beta} \equiv \frac{1}{2i}\log\Big[-\frac{e^{ik_\alpha+ik_\beta} - 2e^{ik_\alpha} + 1}{e^{ik_\alpha+ik_\beta} - 2e^{ik_\beta} + 1}\Big]. \tag{6}$$

The eigenenergy associated to the eigenstate (4) is

$$E = \sum_{\alpha=1}^M(\cos(k_\alpha) - 1). \tag{7}$$

The quasi-momenta k_α are obtained by solving the so-called Bethe equations [29]

$$e^{ik_\alpha L} = \prod_{\beta\neq\alpha}^M\Big[-\frac{1 - 2e^{ik_\alpha} - e^{ik_\alpha+ik_\beta}}{1 - 2e^{ik_\beta} - e^{ik_\alpha+ik_\beta}}\Big]. \tag{8}$$

It is useful to introduce the rapidities $\{\lambda_\alpha\}_{\alpha=1}^M$ as

$$k_\alpha = \pi - 2\arctan(\lambda_\alpha) \mod 2\pi. \tag{9}$$

Taking the logarithm on both sides in (8), and using (9), one obtains the Bethe equations in logarithmic form as

$$\arctan(\lambda_\alpha) = \frac{\pi}{L}J_\alpha + \frac{1}{L}\sum_{\beta\neq\alpha}\arctan\Big(\frac{\lambda_\alpha - \lambda_\beta}{2}\Big), \tag{10}$$

where $-L/2 < J_\alpha \leq L/2$ are the so-called Bethe quantum numbers. The J_α are half-integers and integers for $L - M$ even and odd, respectively.

Finally, one should remark that M-particle eigenstates corresponding to *finite* rapidities are eigenstates with maximum allowed magnetization (highest-weight eigenstates) $S^z_T = L/2 - M = S_T$, with S_T the total spin. Due to the $SU(2)$ invariance of (3), all the states in the same S_T multiplet and different $-S_T \leq S^z_T \leq S_T$ are eigenstates of the XXX chain with the same energy eigenvalue. These eigenstates (descendants) are

obtained by multiple applications of the total-spin lowering operator $S_T^- \equiv \sum_i S_i^-$ on the highest-weight eigenstates. In the Bethe ansatz framework the rapidities of a generic M-particle descendant eigenstate with $S_T^T = L/2 - M'$, with $M' < M$, are obtained by supplementing the M rapidities of the highest-weight state with $M' - M$ infinite rapidities. We anticipate that descendant eigenstates have non-zero overlap with the zero-momentum Néel state (cf. section 3).

2.3. String hypothesis & the Bethe-Gaudin-Takahashi (BGT) equations

In the thermodynamic limit $L \to \infty$ the solutions of the Bethe equations (8) form particular "string" patterns in the complex plane, (string hypothesis) [29, 17]. Specifically, the rapidities forming a "string" of length $1 \leq n \leq M$ (that we defined here as n-string) can be parametrized as

$$\lambda_{n;\gamma}^j = \lambda_{n;\gamma} - i(n-1-2j) + i\delta_{n;\gamma}^j, \qquad j = 0, 1, \ldots, n-1, \tag{11}$$

with $\lambda_{n;\gamma}$ being the real part of the string (string center), γ labelling strings with different centers, and j labelling the different components of the string. In Eq. (11) $\delta_{n;\gamma}^j$ are the string deviations, which typically, i.e., for most of the chain eigenstates, vanish exponentially with L in the thermodynamic limit. Note that real rapidities correspond to strings of unit length (1-strings), i.e., $n = 1$ in Eq. (11).

The string centers $\lambda_{n;\gamma}$ are obtained by solving the so-called Bethe-Gaudin-Takahashi equations

$$2L\theta_n(\lambda_{n;\gamma}) = 2\pi I_{n;\gamma} + \sum_{(m,\beta)\neq(n,\gamma)} \Theta_{m,n}(\lambda_{n;\gamma} - \lambda_{m;\beta}). \tag{12}$$

The generalized scattering phases $\Theta_{m,n}$ read

$$\Theta_{m,n}(x) \equiv \begin{cases} \theta_{|n-m|}(x) + \sum_{r=1}^{(n+m-|n-m|-1)/2} 2\theta_{|n-m|+2r}(x) + \theta_{n+m}(x) & \text{if} \quad n \neq m \\ \sum_{r=1}^{n-1} 2\theta_{2r}(x) + \theta_{2n}(x) & \text{if} \quad n = m \end{cases}$$

with $\theta_\alpha(x) \equiv 2\arctan(x/\alpha)$. Here $I_{n;\gamma}$ are the Bethe-Takahashi quantum numbers associated with $\lambda_{n;\gamma}$. The solutions of (12), and the Bethe states thereof, are naturally classified according to their "string content" $\mathcal{S} \equiv \{s_n\}_{n=1}^M$, with s_n the number of n-strings. Clearly, the constraint $\sum_{n=1}^M n s_n = M$ has to be satisfied. It can be shown that the BGT quantum numbers $I_{n;\gamma}$ associated with the n-strings are integers and half-integers for $L - s_n$ odd and even, respectively. An upper bound for the BGT quantum numbers can be derived as [17]

$$|I_{n;\gamma}| \leq I_n^{(MAX)} \equiv \frac{1}{2}(L - 1 - \sum_{m=1}^M t_{m,n} s_m), \tag{13}$$

where $t_{m,n} \equiv 2\min(n,m) - \delta_{m,n}$. Using the string hypothesis Bethe states energy eigenvalue (7) becomes

$$E = -\sum_{n,\gamma} \frac{2n}{\lambda_{n;\gamma}^2 + n^2}. \tag{14}$$

2.4. Thermodynamic limit

In the thermodynamic limit $L \to \infty$ at fixed finite particle density M/L the solutions of the BGT equations (12) become dense. One then defines the BGT root distributions for the n-strings as $\boldsymbol{\rho} \equiv \{\rho_n(\lambda)\}_{n=1}^{\infty}$, with $\rho_n(\lambda) \equiv \lim_{L\to\infty}[\lambda_{n;\gamma+1} - \lambda_{n;\gamma}]^{-1}$. Thus the BGT equations (12) become an infinite set of coupled non-linear integral equations for the $\rho_n(\lambda)$ as

$$a_n(\lambda) = \rho_n(\lambda) + \rho_n^h(\lambda) + \sum_m (T_{n,m} * \rho_m)(\lambda), \tag{15}$$

where ρ_n^h are the hole-distributions, and the functions $a_n(\lambda)$ are defined as

$$a_n(x) \equiv \frac{1}{\pi}\frac{n}{x^2+n^2}. \tag{16}$$

In (15) $T_{n,m} * \rho_m$ denotes the convolution

$$(T_{n,m} * \rho_m)(\lambda) \equiv \int_{-\infty}^{+\infty} T_{n,m}(\lambda - \lambda')\rho_m(\lambda'), \tag{17}$$

with the matrix $T_{n,m}(x) \equiv \Theta'(x)$ being dfined as

$$T_{m,n}(x) \equiv \begin{cases} a_{|n-m|}(x) + \sum_{r=1}^{(n+m-|n-m|-1)/2} 2a_{|n-m|+2r}(x) + a_{n+m}(x) & \text{if} \quad n \neq m \\ \sum_{r=1}^{n-1} 2a_{2r}(x) + a_{2n}(x) & \text{if} \quad n = m \end{cases}$$

For a generic smooth enough observable $\mathcal{O}$ in the thermodynamic limtit its expectation value is expected to become a functional of the root densities $\boldsymbol{\rho}$ as $\langle\boldsymbol{\rho}|\mathcal{O}|\boldsymbol{\rho}\rangle$.
Moreover, for all the local observables considered in this work the contribution of the different type of strings factorize and one can write

$$\langle\boldsymbol{\rho}|\mathcal{O}|\boldsymbol{\rho}\rangle = \sum_{n=1}^{\infty}\int_{-\infty}^{+\infty} d\lambda \rho_n(\lambda)\mathcal{O}_n(\lambda), \tag{18}$$

with $\mathcal{O}_n(\lambda)$ the ... .

2.5. The conserved charges

The XXX chain exhibits an extensive number of mutually commuting local conserved charges Q_n, with $n \in \mathbb{N}$, i.e.,

$$[Q_n, \mathcal{H}] = 0 \quad \forall n \quad \text{and} \quad [Q_n, Q_m] = 0 \quad \forall n, m. \tag{19}$$

The eigenvalues q_n of the conserved charges over the Bethe eigenstates (cf. (4)) are given as

$$q_{n+1} \equiv \frac{i}{(n-1)!}\frac{d^n}{dy^n}\log\tau(y)\Big|_{y=i}, \tag{20}$$

where y is a spectral parameter and $\tau(y)$ is the Bethe state eigenvalue of the so-called transfer matrix in the Algebraic Bethe Ansatz framework [23]. The analytic expression for $\tau(y)$ in terms of the solutions $\{\lambda_\alpha\}_{\alpha=1}^{M}$ of the Bethe equations (8) is given as

$$\tau(y) \equiv \Big(\frac{y+i}{2}\Big)^L \prod_\alpha \frac{y-\lambda_\alpha-2i}{y-\lambda_\alpha} + \Big(\frac{y-i}{2}\Big)^L \prod_\alpha \frac{y-\lambda_\alpha+2i}{y-\lambda_\alpha}. \tag{21}$$

Interestingly, from (20) one has that the second term in (21) does not contribute to q_n, at least for $n \leq L-2$. For a generic Bethe state q_n is obtained by summing independently the contributions of the BGT roots as

$$q_n = \sum_{k,\gamma} g_{n,k}(\lambda_{k;\gamma}). \tag{22}$$

Using the string hypothesis (11), and (20), (21), one obtains the the first few functions $g_{n,k}$ in terms of the solutions of the BGT equations as

$$\begin{aligned} g_{3,k} &= -\frac{4k\lambda_{k;\gamma}}{(\lambda_{k;\gamma}^2+k^2)^2}, \qquad g_{4,k} = \frac{2k(k^2-3\lambda_{k;\gamma}^2)}{(k^2+\lambda_{k;\gamma}^2)^3} \\ g_{5,k} &= \frac{8k\lambda_{k;\gamma}(k^2-\lambda_{k;\gamma}^2)}{(k^2+\lambda_{k;\gamma}^2)^4}, \quad g_{6,k} = -\frac{2k(5\lambda_{k;\gamma}^4-10k^2\lambda_{k;\gamma}^2+k^4)}{(k^2+\lambda_{k;\gamma}^2)^5}. \end{aligned} \tag{23}$$

Note that q_2 is the Bethe state energy eigenvalue and is given in (14). It is also interesting to observe that $g_{n,k}$ (cf. (23)) is vanishing for infinite BGT roots. This is expected to hold for the generic $g_{n,k}$, i.e., for any n, and it is a consequence of the $SU(2)$ invariance of the conserved charges. Finally, in the thermodynamic limit $L \to \infty$ from (22) one has

$$q_n \to \sum_{k=1}^{\infty} \int_{-\infty}^{+\infty} d\lambda \rho_k(\lambda) g_{n,k}(\lambda), \tag{24}$$

where the BGT root distributions $\rho_k(\lambda)$ are solutions of (15).

3. Overlap between the Bethe states and some initial states

3.1. Néel state overlap

Here we detail the Bethe ansatz results for the overlap of the Bethe states (cf. (4)) with the zero-momentum (one-site shift invariant) Néel state $|N\rangle$ and the Majumdar-Ghosh (MG) $|MG\rangle$ state. We stard discussing the Néel state. This is defined as

$$|N\rangle \equiv \frac{1}{\sqrt{2}}(|N_1\rangle + |N_2\rangle), \tag{25}$$

with $|N_1\rangle \equiv |\uparrow\downarrow\rangle^{\otimes L/2}$, and $|N_2\rangle \equiv |\downarrow\uparrow\rangle^{\otimes L/2}$. Note that $|N_1\rangle = \hat{T}|N_2\rangle$, with $\hat{T}$ the one-site shift operator.

Due to the zero-momentum constraint, only parity-invariant Bethe states can have non-zero Néel overlap [30]. Parity-invariant Bethe states contain only pairs of solutions of the Bethe equations (8) with opposite sign. Here we denote the generic parity-invariant rapidity configuration as $|\{\pm\tilde{\lambda}_\alpha\}_{\alpha=1}^m, n_\infty\rangle$, i.e., considering only positive rapidities. Here m is the number of rapidity pairs. Since the Néel state is not invariant under $SU(2)$ rotations, eigenstates with infinite rapidities can have non-zero Néel overlaps. Here the number of infinite rapidities is denoted as N_∞. Note that one has $M = L/2 = N_\infty + 2m$.

We denote as $n_\infty \equiv N_\infty/L$ the density of infinite rapidities. Finally, the overlap between the Bethe states and the Neel state $|N\rangle$ reads [30, 37]

$$\frac{\langle N|\{\pm\tilde{\lambda}_j\}_{j=1}^m, n_\infty\rangle}{|||\{\tilde{\lambda}_j\}_{j=1}^m, n_\infty\rangle||} = \frac{\sqrt{2}N_\infty!}{\sqrt{(2N_\infty)!}}\left[\prod_{j=1}^m \frac{\sqrt{\tilde{\lambda}_j^2+1}}{4\tilde{\lambda}_j}\right]\sqrt{\frac{\det_m(G^+)}{\det_m(G^-)}}. \tag{26}$$

The matrix $G^\pm$ is defined as

$$G^\pm_{jk} = \delta_{jk}\Big(LK_{1/2}(\tilde{\lambda}_j) - \sum_{l=1}^m K_1^+(\tilde{\lambda}_j,\tilde{\lambda}_l)\Big) + K_1^\pm(\tilde{\lambda}_j,\tilde{\lambda}_k), \qquad j,k=1,\dots,m, \tag{27}$$

where

$$K_1^\pm(\lambda,\mu) = K_1(\lambda-\mu) \pm K_1(\lambda+\mu) \quad \text{with} \quad K_\alpha(\lambda) \equiv \frac{8\alpha}{\lambda^2+4\alpha^2}. \tag{28}$$

Note that our definitions of $K_\alpha(\lambda)$ differs from the one in Ref. [30], due to a factor 2 in the definition of the rapidities (see also (11)).

3.2. The string hypothesis: Reduced Néel overlap formulas

Here we consider the overlap formula for the Neel state (26) in the limit $L\to\infty$, assuming that the rapidities form perfect strings, i.e., $\delta^j_{n;\gamma}=0$ in (11). Then it is possible to rewrite (26) in terms of the string centers $\tilde{\lambda}_{n;\alpha}$ only. Here we restrict ourselves to rapidity configurations with no zero-momentum strings, i.e., with finite string centers. Our results are not valid for zero-momentum strings.

First, we restrict ourselves to parity-invariant string configurations, i.e., considering only strings having positve string centers. We denote the generic parity-invariant string configuration as $\{\tilde{\lambda}_{n;\gamma}\}$, where γ labels the different non-zero string centers, and n is the string length.

It is convenient to first split the indices i,j of $G^\pm_{ij}$ as $i=(n,\gamma,i)$ and $j=(m,\gamma',j)$, with n,m being the length of the strings, γ,γ' labelling the corresponding string centers, and i,j the components of the two strings.

Using (27) and (28), one has that for two consecutive rapidities in the same string, i.e., for $m=n,\gamma=\gamma',|i-j|=2$, the matrices $G^\pm_{jk}$ become ill-defined in the thermodynamic limit. Precisely, since $K_1(\tilde{\lambda}^i_{n;\gamma}-\tilde{\lambda}^{i+1}_{n;\gamma})\sim 1/(\delta^i_{n;\gamma}-\delta^{i+1}_{n;\gamma})$, $G^\pm_{ij}$ diverges in the thermodynamic limit. Importantly, as the same type of divergence occur in both G^+ and G^-, their ratio (cf. (26)), and the overlaps, are finite.

The finite part of the overlaps (26) can be calculated using the same strategy as in Ref. [34, 35] (see also Ref. [30]). The resulting matrix G^+ depends only on the "string center" indices (n,γ) and (m,γ') and it is given as

$$\frac{1}{2}G^+_{(n,\gamma)(m,\gamma')} = \begin{cases} L\theta'_n(\tilde{\lambda}_{n;\gamma}) - \sum\limits_{(\ell,\alpha)\neq(n,\gamma)}\Big[\Theta'_{n,\ell}(\tilde{\lambda}_{n;\gamma}-\tilde{\lambda}_{\ell;\alpha}) \\ \qquad\qquad +\Theta'_{n,\ell}(\tilde{\lambda}_{n;\gamma}+\tilde{\lambda}_{\ell;\alpha})\Big] & \text{if } (n,\gamma)=(m,\gamma') \\ \Theta'_{n,m}(\tilde{\lambda}_{n;\gamma}-\tilde{\lambda}_{m;\gamma'}) + \Theta'_{n,m}(\tilde{\lambda}_{n;\gamma}+\tilde{\lambda}_{m;\gamma'}) & \text{if } (n,\gamma)\neq(m,\gamma') \end{cases} \tag{29}$$

Here $\theta_n'(x) \equiv d\theta_n(x)/dx = 2n/(n^2+x^2)$ and $\Theta'(x) \equiv d\Theta(x)/dx$, with $\Theta(x)$ as defined in (13). Similarly, for G^- one obtains

$$\frac{1}{2}G^-_{(n,\gamma)(m,\gamma')} = \begin{cases} (L-1)\theta_n'(\tilde{\lambda}_{n;\gamma}) - 2\sum_{k=1}^{n-1}\theta_k'(\tilde{\lambda}_{n;\gamma}) & \text{if } (n,\gamma)=(m,\gamma') \\ -\sum_{(\ell,\alpha)\neq(n,\gamma)}\Big[\Theta'_{n,\ell}(\tilde{\lambda}_{n;\gamma}-\tilde{\lambda}_{\ell;\alpha}) + \Theta'_{n,\ell}(\tilde{\lambda}_{n;\gamma}+\tilde{\lambda}_{\ell;\alpha})\Big] & \\ \quad \Theta'_{n,m}(\tilde{\lambda}_{n;\gamma}-\tilde{\lambda}_{m;\gamma'}) - \Theta'_{n,m}(\tilde{\lambda}_{n;\gamma'}+\tilde{\lambda}_{m;\gamma'})) & \text{if } (n,\gamma)\neq(m,\gamma') \end{cases} \tag{30}$$

Note that in presence of zero-momentum strings, additional divergences as $1/(\delta^i_{n;\gamma}+\delta^{i+1}_{n;\gamma})$ appear due to the term $K_1(\lambda+\mu)$ (cf. (28)). It turns out that the treatment of these diverges is a challenging task because it requires the precise knowledge of the string deviations, meaning their dependence on L, for each different type of string. Some results have been provided for small strings in Ref. [27].

Finally, using the string hypothesis and the parity-invariance condition, the multiplicative prefactor in (26) can be simplified. Here we focus on a generic eigenstate of the XXX identified by m pairs of finite rapidities. Note that due to parity invariance and the exclusion of zero-momentum strings, only strings of length up to m are allowed. The "reduced" string content identifying the eigenstate is denoted as $\widetilde{\mathcal{S}} = \{\tilde{s}_1,\dots,\tilde{s}_m\}$, with $\tilde{s}_n$ the number of parity-invariant pairs of n-strings. Using the string hypothesis and (26), one can write

$$\prod_{j=1}^{m}\frac{\sqrt{\tilde{\lambda}_j^2+1}}{4\tilde{\lambda}_j} = \frac{1}{4^m}\prod_{j=1}^{m}\prod_{\ell=1}^{\tilde{s}_j}\left[\frac{\sqrt{j^2+\lambda_{j;\ell}^2}}{\lambda_{j;\ell}}\prod_{k=0}^{\lceil j/2\rceil-1}\frac{(2k)^2+\lambda_{j;\ell}^2}{(2k+1)^2+\lambda_{j;\ell}^2}\right]^{(-1)^j}. \tag{31}$$

3.3. Overlap with the Majumdar-Ghosh state

The Majumdar-Ghosh state $|MG\rangle$ is defined as

$$|MG\rangle \equiv \Big(\frac{|\uparrow\downarrow\rangle - |\downarrow\uparrow\rangle}{\sqrt{2}}\Big)^{\otimes L/2}. \tag{32}$$

The overlap between a generic eigenstate of the XXX chain and the Majumdar-Ghosh state can be obtained from the Néel state overlap in Eq. (26) as [37]

$$\langle MG|\{\pm\lambda_j\}_{j=1}^m\rangle = \prod_{j=1}^{m}\frac{1}{2}\Big(1-\frac{\lambda_j-i}{\lambda_j+i}\Big)\Big(1+\frac{\lambda_j+i}{\lambda_j-i}\Big)\langle N|\{\pm\lambda_j\}_{j=1}^m\rangle \tag{33}$$

The mutliplicative factor in (33), using the string hypothesis is rewritten as

$$\prod_{j=1}^{m}\frac{1}{2}\Big(1-\frac{\lambda_j-i}{\lambda_j+i}\Big)\Big(1+\frac{\lambda_j+i}{\lambda_j-i}\Big) = \tag{34}$$

$$2^m\prod_{j=1}^{m}\prod_{\ell=1}^{\tilde{s}_j}\lambda_{j;\ell}^{1+(-1)^j}(\lambda_{j;\ell}^2+j^2)\prod_{k=0}^{\lfloor j/2\rfloor}\Big[\lambda_{j;\ell}^2+\Big(2k+\frac{1-(-1)^j}{2}\Big)^2\Big]^{-2}$$

3.4. The Néel overlap in the thermodynamic limit

In the thermodynamic limit $L \to \infty$ the expression for the extensive part of the overlap (26) can be written as [30]

$$-\lim_{L\to\infty} \log\left[\frac{\langle N|\{\pm\lambda_j\}_{j=1}^m, n_\infty\rangle}{|||\{\lambda_j\}_{j=1}^m, n_\infty\rangle||}\right] = \frac{L}{2}\Big(n_\infty \log 2 + \sum_{n=1}^{\infty}\int_0^\infty d\lambda \rho_n(\lambda)[g_n(\lambda) + 2n\log(4)]\Big), \quad (35)$$

where

$$g_n(\lambda) = \sum_{l=1}^{n-1}\Big[f_{n-1-2l}(\lambda) - f_{n-2l}(\lambda)\Big], \quad \text{with} \quad f_n(\lambda) = \log\left(\lambda^2 + \frac{n^2}{4}\right), \quad (36)$$

and

$$n_\infty = 1 - 2\sum_{m=1}^{\infty} m\int_{-\infty}^{\infty} d\lambda \rho_m(\lambda). \quad (37)$$

Note that (35) is extensive. Specifically, in Eq. (35) subleading (i.e., subextensive) contributions originating from the determinant ratio $\det_m(G^+)/\det_m(G^-)$ are neglected. Moreover, the term in (35) acts as a driving term in the Quech Action formalism (cf. section 4).

4. Quench Action treatment of the steady state

In the thermodynamic limit the sum over the model eigenstates in (1) can be recast into a functional integral over the BGT root distributions $\boldsymbol{\rho} \equiv \{\rho_n(\lambda)\}_{n=1}^\infty$ (cf. section 2.4) as

$$\sum_\alpha \to \int \mathcal{D}\boldsymbol{\rho} e^{S_{YY}(\boldsymbol{\rho})}. \quad (38)$$

Here $\mathcal{D}\boldsymbol{\rho} \equiv \prod_{n=1}^\infty \mathcal{D}\rho_n(\lambda)$, $\rho_n(\lambda)$, and $S_{YY}(\boldsymbol{\rho})$ is the Yang-Yang entropy, which counts the number of Bethe states leading to the same $\boldsymbol{\rho}$ in the thermodynamic limit. Using (38), for a generic observable $\mathcal{O}$, its diagonal ensemble expectation value (1) becomes

$$\langle\mathcal{O}\rangle = \int \mathcal{D}\boldsymbol{\rho} \exp\Big[2\Re\log\langle\Psi_0|\boldsymbol{\rho}\rangle + S_{YY}(\boldsymbol{\rho})\Big]\langle\boldsymbol{\rho}|\mathcal{O}|\boldsymbol{\rho}\rangle \quad (39)$$

Here it is assumed that in the thermodynamic limit the eigenstate expectation values $\langle\alpha|\mathcal{O}|\alpha\rangle$ (cf. (1)) and the overlaps $\langle\Psi_0|\boldsymbol{\rho}\rangle$ become smooth functionals of the root distributions $\boldsymbol{\rho}$.

The functional integral in (39) can be evaluated in the limit $L \to \infty$ using the saddle point approximation. One has to minimize the functional $\mathcal{F}(\boldsymbol{\rho})$ defined as

$$L\mathcal{F}(\boldsymbol{\rho}) \equiv 2\Re\log\langle\boldsymbol{\rho}|\Psi_0\rangle + S_{YY}(\boldsymbol{\rho}(\lambda)) \quad (40)$$

with respect to $\boldsymbol{\rho}$, i.e., solving $\delta\mathcal{F}(\boldsymbol{\rho})/\delta\boldsymbol{\rho}|_{\boldsymbol{\rho}=\boldsymbol{\rho}^*} = 0$, under the constraint that the thermodynamic BGT equations (15) hold. Finally, one obtains from (39) that in the thermodynamic limit

$$\langle\mathcal{O}\rangle = \langle\boldsymbol{\rho}^*|\mathcal{O}|\boldsymbol{\rho}^*\rangle. \quad (41)$$

Remarkably, for the quench with initial state the Néel state $|\Psi_0\rangle = |N\rangle$ the saddle point root distributions $\rho_n^*(\lambda)_{n=1}^{\infty}$ can be obtained analytically [30]. The first few are given as

$$\rho_1^*(\lambda) = \frac{8(4+\lambda^2)}{\pi(19+3\lambda^2)(1+6\lambda^2+\lambda^4)} \tag{42}$$

$$\rho_2^*(\lambda) = \frac{8\lambda^2(9+\lambda^2)(4+3\lambda^2)}{\pi(2+\lambda^2)(16+14\lambda^2+\lambda^4)(256+132\lambda^2+9\lambda^4)} \tag{43}$$

$$\rho_3^*(\lambda) = \frac{8(1+\lambda^2)^2(5+\lambda^2)(16+\lambda^2)(21+\lambda^2)}{\pi(19+3\lambda^2)(9+624\lambda^2+262\lambda^4+32\lambda^6+\lambda^8)(509+5\lambda^2(26+\lambda^2))}. \tag{44}$$

5. Néel overlaps: The role of the zero-momentum strings Bethe states

In this section we discuss generic features of the overlaps between the eigenstates (Bethe states) of the Heisenberg spin chain and the Néel state (cf. (25)). We exploit the Bethe ansatz solution of the chain (see section 2) as well as exact results for the Néel overlaps (see section 3). We focus on finite chains with $L \lesssim 40$ sites, considering, for any L, the full Hilbert space of the chain. The Bethe states having, in principle, non zero Néel overlap are the so-called parity-invariant Bethe states (see section 3). We denote their total number as Z_{Neel}. Crucially, here we restrict ourselves to the subset of parity-invariant Bethe states corresponding to solutions of the Bethe-Gaudin-Takahashi (BGT) equations (12) that do not contain zero-momentum strings. We denote the total number of these eigenstates as $\widetilde{Z}_{Neel}$. Both Z_{Neel} and $\widetilde{Z}_{Neel}$ are given in terms of the chain length L by simple combinatorial formulas that we provide.

Interestingly, the fraction of eigenstates with no zero-momentum strings, i.e., $\widetilde{Z}_{Neel}/Z_{Neel}$, is vanishing as $L^{-1/2}$ in the thermodynamic limit, meaning that zero-momentum strings eigenstates are dominant, at least in number, for large chains. This has dramatic consequences, for instance, at the level of the overlap sum rules for the local conservation laws of the model. Precisely, although the sum rules are fixed by the initial (Néel) state expectation value of the local charges, we observe striking violations for any finite chain. Moreover, all the sum rules exhibit vanishing behavior as $L^{-1/2}$ upon increasing the chain size, reflecting the same vanishing behavior as $\widetilde{Z}_{Neel}/Z_{Neel}$. A similar scenario holds for the overlaps with the Majumdar-Ghosh state, where, however, excluding the zero-momentum strings leads to a $1/L$ behavior. This demonstrates that for finite chains the physical effects of zero-momentum strings eigenstates are not negligible.

5.1. Néel overlap distribution function: Overview

Here we overview the Bethe ansatz results for the Néel overlaps with the eigenstates of the XXX chain. The total number of partiy-invariant eigenstates Z_{Neel} having, in principle, non-zero Néel overlap is given as

$$Z_{Neel} = 2^{\frac{L}{2}-1} + \frac{1}{2}B\Big(\frac{L}{2},\frac{L}{4}\Big) + 1, \tag{45}$$

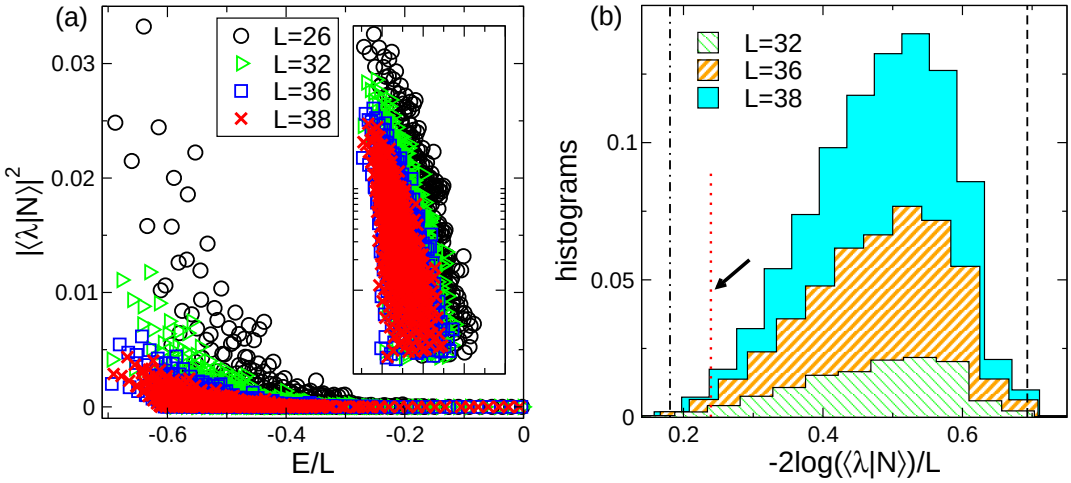

Figure 1. Néel overlaps with the eigenstates of the Heisenberg spin chain: Numerical results obtained from the full scanning of the chain Hilbert space. Eigenstates corresponding to zero-momentum strings are escluded. (a) Squared overlaps $|\langle\lambda|N\rangle|^2$ plotted as function of the eigenstates energy density E/L. Here $|\lambda\rangle$ denotes the generic eigenstate. The data are for chains with length $26 \leq L \leq 38$. The inset is to highlight the exponential decay as a function of E/L. Note the logarithmic scale on the y axis. (b) Overlap distribution function: Histograms of $-2\log\langle\lambda|N\rangle/L$. The y-axis is rescaled by a factor 10^5 for convenience. The dash-dotted and dashed vertical lines are the Néel overlaps with the XXX chain ground state and the ferromagnetic state, respectively. The dotted line (see the arrow) is the result obtained using the quench action approach.

with $B(n,m) \equiv n!/(m!(n-m)!)$ the Newton binomial. The proof of (45) is obtained by counting all the parity-invariant BGT quantum number configurations, and it is reported in Appendix A. Note that Z_{Neel} provides only an upper bound for the number of eigenstates with non-zero Néel overlap, as it is clear from the exact diagonalization results shown in Table C1. This is because parity-invariant eigenstates with a single zero-momentum even-length string, which are included in (45), have identically zero Néel overlap [30]. This is not related to the symmetries of the Néel state, but to the "accidental" vanishing of the prefactor in the overlap formula (26). Finally, after excluding the zero-momentum strings eigenstates, the total number of remaining eigenstates $\widetilde{Z}_{Neel}$, which are the ones considered here, is given as (see Appendix B for the proof)

$$\widetilde{Z}_{Neel} = B\Big(\frac{L}{2}, \frac{L}{4}\Big). \tag{46}$$

An overview of generic features of the overlaps is given in Figure 1 (a) plotting the squared Néel overlaps $|\langle\lambda|N\rangle|^2$ with the XXX chain eigenstates $|\lambda\rangle$ versus the energy density E/L. The figure shows results for chains with $26 \leq L \leq 38$ sites. The data are obtained by generating all the relevant parity-invariant BGT quantum numbers, and solving the associated BGT equations (12), to obtain the rapidities of XXX chain eigenstates. The Néel overlaps are calculated numerically using (26). Note that for

$L = 38$ from (46) the total number of overlap shown in the Figure is $\widetilde{Z}_{Neel} \sim 10^5$. Clearly, the overlaps decay exponentially as a function of L, as expected. Moreover, at each finite L a rapid decay as a function of E/L is observed. The inset of Figure 1 (a) suggests that the decay is exponential. Complementary information about the overlaps is shown in Figure 1 (b) plotting the histograms of $\kappa \equiv -2\log|\langle\lambda|N\rangle|/L$ (overlap distribution function). Larger values of κ, correspond to a faster decay with L of the overlaps. The factor $1/L$ in the definition takes into account that the Néel overlaps vanish exponentially as $|\langle\lambda|N\rangle|^2 \propto e^{-\kappa L}$ in the thermodynamic limit. Note that κ is the driving term in the quench action approach (cf (35)). As expected, from Figure 1 (b) one has that the majority of the XXX chain eigenstates give small Néel overlap (note the maximum at $\kappa \sim 0.5$). Interestingly, the data suggest that with $0.18 \lesssim \kappa \lesssim 0.7$. The vertical dash-dotted line in the figure is the κ obtained from the Néel overlap of the ground state of the XXX chain in the thermodynamic limit. This is derived using the ground state root distribution $\rho_1(\lambda) \propto 1/\cosh(\pi\lambda)$ and (35). On the other hand, the vertical dashed line denotes the Néel overlap $\sim 2/B(L, L/2)$ of the $S_z = 0$ component of the ferromagnetic multiplet, which is at the top of the chain energy spectrum. Finally, the vertical dotted line in Figure 1 (b) shows the quench action result for κ in the thermodynamic limit. This is obtained by using (35) and the saddle point root distributions ρ_n^* (cf. (42)-(44) for the results up to $n = 3$). Note that κ does not coincide with the peak of the overlap distribution function, as expected, due to the effect of the driving term (35) in the quench action approach.

5.2. Néel overlap sum rules

Here we illustrate the effect of the zero-momentum strings eigenstates on the Néel overlap sum rules. We focus on the "trivial" sum rule, i.e., the normalization of the Néel state

$$\langle N|N\rangle = \sum_{\lambda} |\langle\lambda|N\rangle|^2 = 1. \tag{47}$$

We also consider the Néel expectation value of the local conserved charge Q_n of the XXX chain (see subsection 2.5), which provide the additional sum rules

$$Q_n^{(0)} = \langle N|Q_n|N\rangle = \sum_{\lambda} |\langle\lambda|N\rangle|^2 Q_n(\lambda) \quad \text{with} \quad n \in \mathbb{N}, \tag{48}$$

where $Q_n(\lambda)$ are the charges eigenvalues over the generic Bethe state $|\lambda\rangle$ (cf. (22) and (23)). In both (47) and (48) the sum are restricted to the eigenstates with containing no zero-momentum strings. In (48) $Q_n^{(0)}$ is the charge expectation value over the initial state, i.e., the Néel state, which has been calculated in Ref. [43]. Due to the locality of Q_n, the translational invariance of the initial state, and the periodic boundary conditions, the density $Q_n^{(0)}/L$ does not depend on the chain size. For the Néel state, $Q_n^{(0)}$ can be calculated directly in the thermodynamic limit using (24) and the root distributions $\boldsymbol{\rho}^*$ (cf. (42)-(44)).

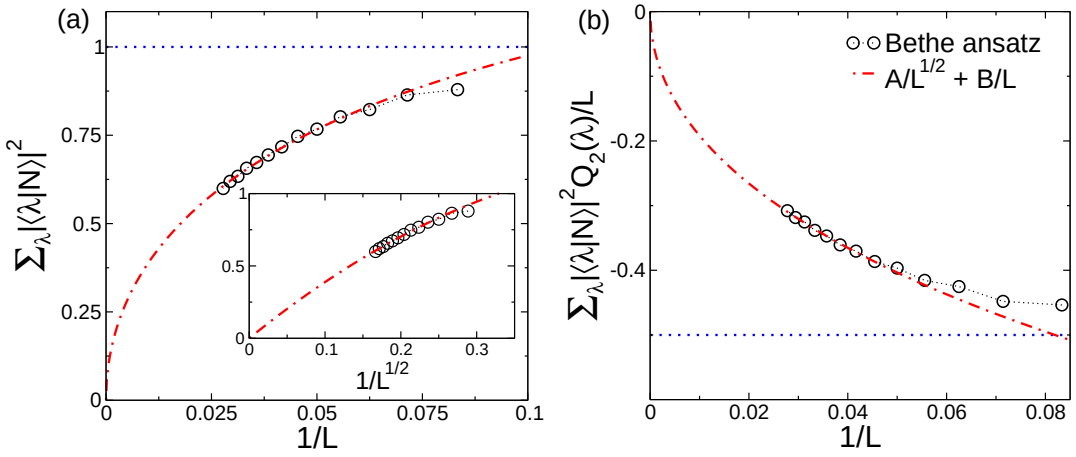

Figure 2. Overlap sum rules for the Néel state $|N\rangle$: The role of the zero-momentum strings. (a) The overlap sum rule $\sum_\lambda |\langle\lambda|N\rangle|^2 = 1$. Here $|\lambda\rangle$ are the eigenstates of the XXX chain. The x-axis shows the inverse chain length $1/L$. The circles are Bethe ansatz results for chains up to $L = 38$. The data are obtained by a full scanning of the chain Hilbert space. Eigenstates corresponding to zero-momentum strings are excluded. The dotted line is the expected result at any L. The data are compatible with a vanishing behavior in the thermodynamic limit. The dash-dotted line is a fit to $A/L^{1/2} + B/L$, with A, B fitting parameters. Inset: The same data as in the main Figure now plotted versus $1/L^{1/2}$. (b) The same as in (a) for the energy sum rule $\sum_\lambda |\langle\lambda|N\rangle|^2 Q_2(\lambda) = Q_2^{(0)}$, with $Q_2(\lambda)$ the energy of the eigenstate $|\lambda\rangle$ and $Q_2^{(0)}/L = -1/2$ the Néel state energy density (dotted line in the Figure).

The sum rules (47) and (48) (for $n = 2$, i.e., the energy sum rule), are shown in Figure 2 (a) and (b), respectively. Note that $Q_2^{(0)}/L = -1/2$ in (48) (horizonthal dotted line in Figure 2 (b)). The circles in Figure 2 (a) are the Bethe ansatz results excluding the zero momentum strings. The data are the same as in Figure 1. The sum rules are plotted against the inverse chain length $1/L$, for $L \leq 38$.

Clearly, both the sum rules are violated, due to the exclusion of the to zero-momentum strings. Moreover, in both Figure 2 (a) and (b) the data suggest a vanishing behavior upon increasing L. The dash-dotted lines in the Figures are fits to $A/L^{1/2} + B/L$, with A, B fitting parameters. Interestingly, the behavior as $\propto L^{-1/2}$ of the sum rules reflects that of the fraction of non-zero momentum string eigenstates in the thermodynamic limit $\widetilde{Z}_{Neel}/Z_{Neel}$. Specifically, from (45) and (46) it is straightforward to derive that in the thermodynamic limit

$$\frac{\widetilde{Z}_{Neel}}{Z_{Neel}} \propto \frac{4}{\sqrt{\pi L}}. \tag{49}$$

It is interesting to observe that the large L behavior as $L^{-1/2}$ is not generic, meaning that it depends on the initial state $|\Psi_0\rangle$. This is illustrated in Figure 3, focusing on the Majumdar-Ghosh (MG) state. As for the Néel state, only parity-invariant eigenstates can have non-zero Majumdar-Ghosh overlap. Their total number Z_{MG} (cf. (A.17)) is

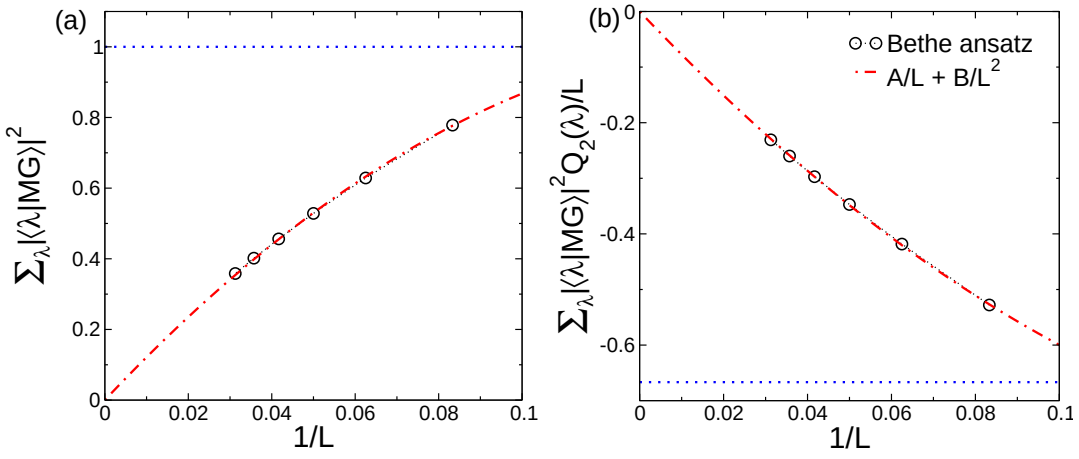

Figure 3. Overlap sum rules for the Majumdar-Ghosh state $|MG\rangle$: The role of the zero-momentum strings. (a) The sum rule $\sum_\lambda |\langle\lambda|MG\rangle|^2 = 1$, with $|\lambda\rangle$ the eigenstates of the XXX chain. The x-axis plots the inverse chain length $1/L$. The circles are Bethe ansatz results for chains up to $L = 32$. The results are obtained by a full scanning of the chain Hilbert space. Eigenstates corresponding to zero-momentum strings are excluded. The dash-dotted line is a fit to $A/L + B/L^2$, with A, B fitting parameters. (b) The same as in (a) for the energy sum rule $\sum_\lambda |\langle\lambda|MG\rangle|^2 Q_2(\lambda) = Q_2^{(0)}$, with $Q_2(\lambda)$ the energy of $|\lambda\rangle$ and $Q_2^{(0)}/L = -2/3$ the Majumdar-Ghosh energy density (dotted line in the Figure).

given as

$$Z_{MG} = B\Big(\frac{L}{2} - 1, \frac{L}{4} - 1\Big) + B\Big(\frac{L}{2} - 1, \frac{L}{4} - 1\Big). \tag{50}$$

Note that at any size L one has $Z_{MG} < Z_{Neel}$. This is due to the fact that the Majumdar-Ghosh state is invariant under $SU(2)$ rotations, since it contains only spin singlets, and it has non-zero overlap only with the $S^z_T = 0$ sector of the XXX chain spectrum. The total number of parity-invariant eigenstates that contain no zero-momentum strings $\widetilde{Z}_{MG}$ is instead (cf. (B.7))

$$\widetilde{Z}_{MG} = B\Big(\frac{L}{2}, \frac{L}{4}\Big) - B\Big(\frac{L}{2}, \frac{L}{4} - 1\Big). \tag{51}$$

Panels (a) and (b) in Figure 3 plot the sum rules (47) and (48) for the Majumdar-Ghosh state. The data are obtained using the analytic results for the overlaps in subsection 3.3. The expected value for the energy density sum rule is $Q_2^{(0)} = -2/3$ (horizonthal dotted line in Figure 3 (b)). Similar to Figure 2, due to the exclusion of the zero-momentum strings, the sum rules are violated, exhibiting vanishing behavior in the thermodynamic limit. However, in contrast with the Néel case, one has the behavior as $1/L$, as confirmed by the fits (dash-dotted lines in Figure 3). Similar to the Néel case, the vanishing of the sum rules in the thermodynamic limit reflects the behavior of $\widetilde{Z}_{MG}/Z_{MG}$ as (see (50) and (51))

$$\frac{\widetilde{Z}_{MG}}{Z_{MG}} = \frac{4}{4 + L}. \tag{52}$$

6. Monte Carlo implementation of the quench action approach

Here, by generalizing the results presented in Ref. [28], we present a Monte Carlo implementation of the quench action approach for Néel quench in the XXX chain. The key idea is to sample the eigenstates of the finite-size XXX chain with the diagonal ensemble, equivalently the quench action, probability distribution, given in (39). Importantly, we consider a truncated Hilbert space, restricting ourselves to the eigenstates corresponding to solutions of the BGT equations with no zero-momentum strings. Our main physical result is that, despite this restriction, the remaining eigenstates contain enough information to correctly reproduce the post-quench thermodynamic behavior of the XXX chain.
In subsection 6.1 we detail the Monte Carlo algorithm. In subsection 6.2 we numerically demonstrate that after the Monte Carlo "resampling" the Néel sum rules (48) are restored, in the thermodynamic limit. The Hilbert space truncation is reflected only in $\propto 1/L$ finite-size corrections to the sum rules. In the Bethe ansatz language our results mean that the eigenstates sampled by the Monte Carlo approach the quench action representative state in the thermodynamic limit. This is explicitly demonstrated here by numerically extracting the quench action root distributions $\boldsymbol{\rho}^*$ (cf. (42)-(44)). The numerical results are found in remarkable agreement with the quench action.

6.1. The quench action Monte Carlo algorithm

The Monte Carlo procedure starts with a randomly selected parity-invariant eigenstate (Bethe state) of the XXX chain, in the sector with zero magnetization, i.e., $M = L/2$ particles. Due to the fact that the Néel state is not invariant under $SU(2)$ rotations, in order to characterize the Bethe states one has to specify the number N_∞ of infinite rapidities. The number of remaining particles corresponding to finite roots M' is $M' = L/2 - N_\infty$. The state is identified by a parity-invariant BGT quantum number configuration that we denote as $\mathcal{C}$. Due to the parity-invariance and the zero-momentum strings being excluded, $\mathcal{C}$ is identified by the number m' of parity-invariant rapidities $\{\pm\lambda_j\}_{j=1}^{m'}$. The string content associated with the state is denoted as $\widetilde{\mathcal{S}} = \{\tilde{s}_1, \ldots, \tilde{s}_{m'}\}$, where $\tilde{s}_n$ is the number of pairs of n-strings. The Monte Carlo procedure generates a new parity-invariant eigenstate of the XXX chain, and it consists of four steps:

(1) Choose a new number of finite-momentum particles M'' and of parity-invariant rapidity pairs $m'' \equiv M''/2$ with probability $\mathcal{P}(M'')$ as

$$\mathcal{P}(M'') = \frac{\widetilde{Z}'_{Neel}(L, M'')}{\widetilde{Z}_{Neel}(L)}, \tag{53}$$

where $\widetilde{Z}_{Neel}(L)$ is defined in (46), and $\widetilde{Z}'_{Neel}$ is the number of parity-invariant eigenstates with no zero-momentum strings in the sector with fixed particle number M'' (cf. (B.6) for the precise expression).

(2) Choose a new string content $\widetilde{\mathcal{S}}' \equiv \{\tilde{s}'_1, \ldots, \tilde{s}'_{m''}\}$ with probability $\mathcal{P}'(M'', \widetilde{\mathcal{S}}')$

$$\mathcal{P}'(M'', \widetilde{\mathcal{S}}') = \frac{1}{\widetilde{Z}'_{Neel}(L, M'')} \prod_{n=1}^{m''} B\Big(\frac{L}{2} - \sum_{l=1}^{m''} t_{nl}\tilde{s}'_l, \tilde{s}'_n\Big), \tag{54}$$

where the matrix t_{nl} is defined in (13).

(3) Generate a new parity-invariant quantum number configuration $\mathcal{C}'$ compatible with the $\widetilde{\mathcal{S}}'$ obtained in step (2). Solve the corresponding BGT equations (12), finding the rapidities $\{\pm\lambda'_j\}_{j=1}^{m''}$ of the new parity-invariant eigenstate.

(4) Calculate the Néel overlap $\langle\{\pm\lambda'_j\}_{j=1}^{m''}|N\rangle$ for the new eigenstate, using (26) (29) (30) and (31). Accept the new eigenstate with the quench action Metropolis probability

$$\mathcal{P}''_{\lambda\to\lambda'} = \mathrm{Min}\Big\{1, \exp\Big(-2\Re(\mathcal{E}' - \mathcal{E})\Big)\Big\}, \tag{55}$$

where $\mathcal{E}' \equiv -\log\langle\{\pm\lambda'_j\}_{j=1}^{m''}|N\rangle$, $\mathcal{E} \equiv -\log\langle\{\pm\lambda_j\}_{j=1}^{m''}|N\rangle$, and $\Re$ denoting the real part.

Note that while the steps 1-3 account for the string content and particle number probabilities of the parity-invariant states, step 4 assigns to the different eigenstates the right quench action, equivalently diagonal ensemble, probability.
For a generic observable $\mathcal{O}$, its quench action, or diagonal ensemble average, $\langle\mathcal{O}\rangle$ is obtained from the Monte Carlo simulation as the arithmetic average of the eigenstates expectation values $\langle\lambda|\mathcal{O}|\lambda\rangle$, with $|\lambda\rangle$ the eigenstates sampled by the Monte Carlo, as

$$\langle\mathcal{O}\rangle = \frac{1}{N_{mcs}} \sum_{\lambda} \langle\lambda|\mathcal{O}|\lambda\rangle. \tag{56}$$

Here N_{mcs} being the total number of Monte Carlo steps. Note that, as usual in Monte Carlo, some initial steps have to be neglected to ensure thermalization. Note that (56) can be used for any observable $\mathcal{O}$ for which the the Bethe state expectation value $\langle\lambda|\mathcal{O}|\lambda\rangle$ (form factor) is known.

6.2. The Néel overlap sum rules: Monte Carlo results

The validity of the Monte Carlo approach for simulating the quench action is demonstrated in Figure 4 (a)-(d). The Figure focuses on the Néel overlap sum rules for the conserved charges densities Q_2/L and Q_4/L (cf. subsection 2.5 for the definition of the charges, and (48) for the associated sum rules). We also consider the corresponding fluctuations $\sigma^2(Q_n)$, which are defined as

$$\sigma^2(Q_n) \equiv \langle N|Q_n^2|N\rangle - \langle N|Q_n|N\rangle^2 = \sum_{\lambda} |\langle N|\lambda\rangle|^2 Q_n^2(\lambda) - \Big(\sum_{\lambda} |\langle N|\lambda\rangle|^2 Q_n(\lambda)\Big)^2. \tag{57}$$

Note that in both (48) and (57) the sum is now over the eignestates $|\lambda\rangle$ sampled by the Monte Carlo. Panel (a) and (b) in Figure 4 plot the sum rules for the energy density Q_2/L, and its density of fluctutations $\sigma^2(Q_2)/L$. It is straightforward to derive the Néel expectation value of the energy density fluctuations as $\sigma(Q_2)/L = 1/4$. This is shown as dash-dotted line in Figure 4 (b).

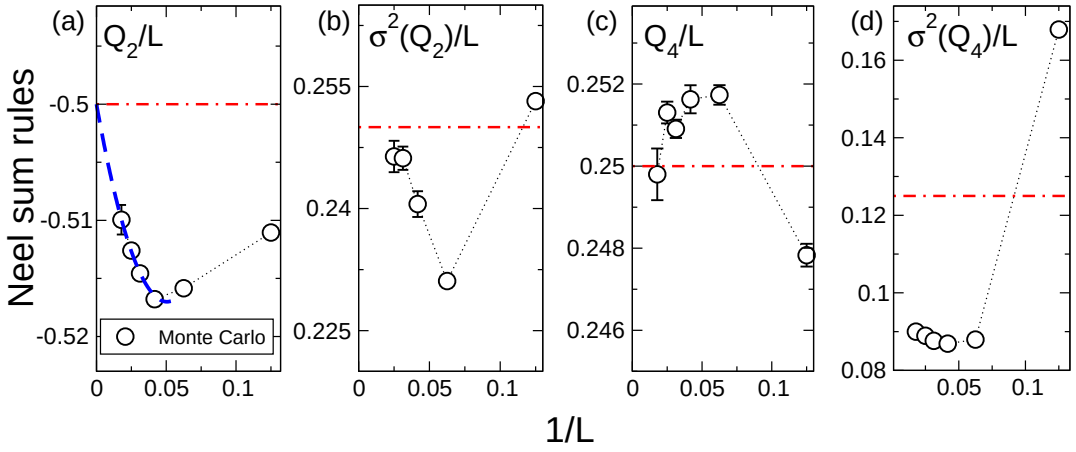

Figure 4. The overlap sum rules for the Néel state $|N\rangle$ in the Heisenberg spin chain: Numerical results obtained by the Monte Carlo sampling of the chain Hilbert space. In all panels the x axis shows the inverse chain length $1/L$ (a) The energy sum rule $\sum_\lambda |\langle N|\lambda\rangle|^2 Q_2(\lambda)/L = Q_2^{(0)}$, with $|\lambda\rangle$ the generic eigenstate of the XXX chain, $Q_2(\lambda)/L$ the associated energy density, and $Q_2^{(0)} = -1/2$ the Néel energy density. The symbols are Monte Carlo data. The dash-dotted line is the expected result $Q_2^{(0)}$. The dashed line is a fit to the behavior $-1/2 + A/L + B/L^2$, with A, B fitting parameters. (b) The Néel sum rule for the energy fluctuations $\sigma^2(Q_2)$ (cf. (57) for the definition). The horizontal line is the expected result $1/4$. (c)(d) Same as in (a)(b) for the charge Q_4 and its fluctuations.

The circles in the Figure are Monte Carlo data obtained using the procedure outlined in 6.1 for the Heisenberg chain with $L \leq 56$ sites. The data correspond to Monte Carlo simulations with $N_{mcs} \sim 10^7$ Monte Carlo steps (mcs). For the largest chain size $L = 56$ we used $N_{mcs} \sim ....$ In all panels the x-axis shows the inverse chain length $1/L$.
Clearly, the Monte Carlo data suggest that in the thermodynamic limit the Néel overlap sum rules (48) are restored, while violations are present for finite chains. This numerically confirms that the truncation of the Hilbert space, i.e., removing the zero-momentum strings, gives rise only to scaling corrections, while the thermodynamic behavior after the quench is correctly reproduced. Note that the data in panel (a) suggest the behavior $\propto 1/L$ for the scaling corrections, as confirmed by the fit to $-1/2 + A/L + b/L^2$ (dashed line in the Figure), with A, B fitting parameters. The same behavior should be expected for the energy fluctuations $\sigma^2(Q_2)$ (panel (b) in the Figure), although the data suggest that this asymptotic behvior sets in for $L \gg 56$.
Similarly, panels (c) and (d) in Figure 4 plot the charge density Q_4/L and its fluctuations $\sigma^2(Q_4)/L$. While for Q_4/L the Monte Carlo data for $L = 48$ are already compatible with the expected result $Q_4/L = 1/4$ in the thermodynamic limit, $\sigma^2(Q_4)$ exhibits large scaling corrections. This could be attributed to fact that the support of Q_n, i.e., the number of sites where the operator acts non trivially, increases linearly with n (see [44] for the precise expression).

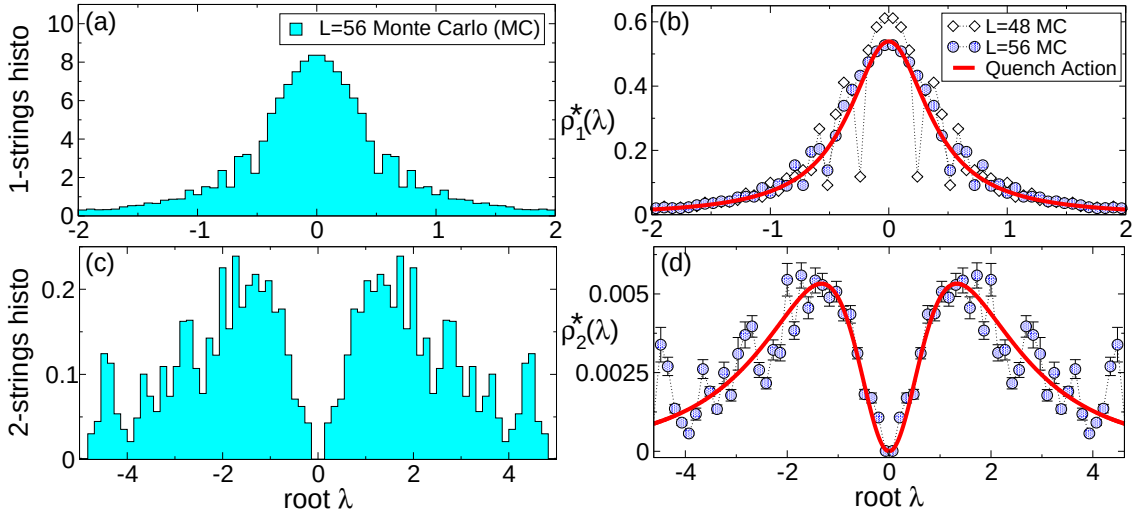

Figure 5. The quench action root distributions $\rho_1^*(\lambda)$ and $\rho_2^*(\lambda)$ for the 1-strings and 2-strings, respectively: Monte Carlos results. (a) The histograms of the 1-string Bethe-Gaudin-Takahashi (BGT) roots λ sampled in the Monte Carlo. The data are for a chain with $L = 56$ sites and a Monte Carlo history with $N_{mcs} \sim 10^7$ Monte Carlo steps. The y-axis is divided by a factor 10^6 for convenience. The width of the histogram bin is $\Delta\lambda \sim 0.07$. (c) The same as in (a) for the 2-string roots. (b) The 1-string root distribution $\rho_1^*(\lambda)$ plotted versus λ for two chains with $L = 48$ and $L = 56$ (diamond and circles, respectively). The full line is the quench action analytic result in the thermodynamic limit. (d) The same as in (b) for the 2-string root distribution $\rho_2^*(\lambda)$. In both (b) and (d) the oscillations are finite-size effects, whereas the error bars are the statistical Monte Carlo errors.

6.3. Extracting the quench action root distributions

The BGT root distributions corresponding to the quench action steady state (cf. (42)-(44)) $\boldsymbol{\rho^*} = \{\rho_n^*(\lambda)\}_{n=1}^{\infty}$ can be extracted from the Monte Carlo simulation, as it has been done in Ref. [28] for the Generalized Gibbs Ensemble (GGE) representative state.
For the local observables considered here, in each eigenstate expectation value $\langle\lambda|\mathcal{O}|\lambda\rangle$ in (56) one can isolate the contribution of the different string sectors as

$$\langle\lambda|\mathcal{O}|\lambda\rangle = \sum_{n,\gamma} \mathcal{O}_n(\lambda_{n;\gamma}), \tag{58}$$

where $\mathcal{O}_n$ is the contribution of the BGT n-strings to the expectation value of $\mathcal{O}$, and $\pm\lambda_{n;\gamma}$, with γ labeling the different n-strings, are the solutions of the BGT equations (12) identifying the Bethe state $|\lambda\rangle$. By comparing (56) and (41) one obtains that in the limit $L, N_{mcs} \to \infty$

$$\lim_{N_{mcs}\to\infty} \frac{1}{N_{mcs}} \sum_{\lambda_{n;\gamma}} \mathcal{O}_n(\lambda_{n;\gamma}) \xrightarrow{L\to\infty} \langle\boldsymbol{\rho^*}|\mathcal{O}|\boldsymbol{\rho^*}\rangle \equiv \sum_n \int_{-\infty}^{+\infty} d\lambda \rho_n^*(\lambda)\mathcal{O}_n(\lambda). \tag{59}$$

This suggests that the histogram of the n-strings BGT roots sampled in the Monte Carlo converges in the thermdynamic limit to the saddle point root distribution $\rho_n^*(\lambda)$.

This is demonstrated numerically in Figure 5 considering $\rho_1^*(\lambda)$ (panels (a)(b)) and $\rho_2^*(\lambda)$ (panel (c)(d)). The histograms correspond to Monte Carlo data for $L = 48$ and $L = 56$ sites. Panel (a) and (c) show the histograms of the 1-string and 2-string BGT roots sampled in the Monte Carlo. The y-axis is rescaled by a factor 10^6 for convenience. The width of the histogram bins $\Delta\lambda$ is $\Delta\lambda \approx 0.02$ and $\Delta\lambda \approx 0.001$ for $\rho_1(\lambda)$ and $\rho_2(\lambda)$, respectively. The histogram fluctuations are due both to the finite statistics (finite N_{mcs}) and to the finite size of the chain.

The extracted quench-action root distributions $\rho_1^*(\lambda)$ and $\rho^*(\lambda)$ are shown in panels (b) and (d). The data are the same as in panel (a)(c). The normalization of the distributions is chosen such as to match the analytical results from (42) and (43), i.e., $\int d\lambda \rho_1^*(\lambda) \approx 0.31$ and $\int d\lambda \rho_2^*(\lambda) \approx 0.015$. The Monte Carlo error bars shown in the Figure are obtained with a standard jackknife analysis [45, 46]. The continuous lines are the expected analytic result in the thermodynamic limit (cf. (42) (43)).

Clearly, the Monte Carlo data for $\rho_1^*(\lambda)$ are in excellent agreement with (42) in the whole range $-2 \leq \lambda \leq 2$ considered. The statistical error bars are smaller than the symbol size. The oscillating (with λ) corrections visible at $|\lambda| \sim 0.5$ are lattice effects, which decrease with the chain size (see the data for $L = 48$). Much larger finite-size effects are observed for $\rho_2^*(\lambda)$ (panel (d) in the Figure). The corrections are larger on the tails of the root distribution. Moreover, the Monte Carlo error bars are clearly visible. This is due to the fact that since $\int d\lambda \rho_2^*(\lambda) / \sum_n \int d\lambda \rho_n^*(\lambda) \approx 0.04$, the Monte Carlo statistics available to estimate $\rho_2^*(\lambda)$ is effectively reduced as compared to $\rho_1^*(\lambda)$. Finally, we numerically checked that these corrections are even larger for the 3-strings, and much larger chains would be needed to extract $\rho_3^*(\lambda)$.

7. Conclusions

We presented a Monte Carlo implementation of the quench action method for integrable spin chains. We focused on the spin-1/2 isotropic Heisenberg (XXX) chain, considering the quench from the zero-momentum Néel state. The method is similar to the Monte Carlo approach developed in Ref. [28] to simulate the Generalized Gibbs Ensemble (GGE) in integrable models. The key idea is the Monte Carlo sampling of the chain Hilbert space with the quench action probability distribution given in (2).

The approach heavily relies on the knowledge of the overlaps between the pre-quench Néel state $|N\rangle$ and the chain eigenstates, which have been obtained recently [37, 30, 41, 32, 31, 47]. Moreover, the method is based on the detailed knowledge of the Hilbert space structure of the model provided by the Bethe ansatz formalism, in particular, on the so-called string hypothesis, and on the Bethe-Gaudin-Takahashi (BGT) equations. Although the approach is devised for finite-size systems, thermodynamic quantities can be extracted using finite-size scaling. Importantly, we restricted ourselves to a truncated Hilbert space, excluding the chain eigenstates containing zero-momentum strings. The reason is that zero-momentum strings lead to singularities in the Néel overlap formulas, which are tricky to deal with in the framework of the string hypothesis. Note that

for the same reason the zero-momentum strings are neglected in the quench action approach [30] as well, although it has been argued that their effect should be irrelevant in the thermodynamic limit [30].

In order to understand the effect of the zero-momentum strings in *finite* chains we first investigated the overlap distribution, including *all* the eigenstates with no zero-momentum strings, for chains up to $L = 38$ sites. Interestingly, the total number of eigenstates having, in principle, non-zero Néel overlap is given in terms of the chain length by a simple combinatorial formula that we provided. Additional combinatorial formulas are provided for the case without zero-momentum strings, or at fixed particle number (i.e., magnetization), or fixed "string content" of the eigenstates. Surprisingly, for any finite chain the majority of eigenstates contain zero-momentum strings. Moreover, the fraction of eigenstates with nonzero-momentum strings vanishes as $L^{-1/2}$ in the thermdodynamic limit. This is reflected in the Néel overlap sum rules for the local conserved charges of the model. Although for any chain size their value is fixed by the Néel state expectation value, violations of the sum rules are observed, due to the Hilbert space truncation. Moreover, we numerically observed that the sum rules vanish as $L^{-1/2}$ in the thermodynamic limit. This behavior reflects the vanishing of the fraction of eigenstates with no zero-momentum strings, confirming that their contribution cannot be trivially neglected. This behavior as$L^{-1/2}$, however, is not generic, but it depends on the pre-quench initial state. This was demonstrated by considering the quench from the Majumdar-Ghosh state. We observed that the sum rules vanish as $1/L$, again reflecting the vanishing as $1/L$ of the fraction of eigenstates with no zero-momentum strings.

Next we presented a Monte Carlo implementation of the quench action method. We numerically demonstrated the validity of the approach, focusing on the Néel overlap sum rules for the local conserved quantities of the XXX chain. Although for finite chains violations of the sum rules are present, their effect decays as $1/L$ upon increasing the chain size, meaning that overlap sum rules are restored in the thermodynamic limit. This implies that the only effect of the Hilbert space truncation is to give rise to scaling corrections. Physically, this means that the remaining eigenstates after the Hilber space truncation contain enough information about the post-quench thermodynamic behavior of the model. Finally, following Ref. [28] we extracted from the Monte Carlo the quench action BGT root distributions. Although finite-size oscillating corrections are present, already for relatively small chains with $L = 56$ sites, the first two BGT root distributions are in impressive agreement with the analytic result in the thermodynamic limit.

Appendix A. Eigenstates with nonzero Néel overlap: eigenstates counting and string content

Here we prove that the total number of eigenstates with Néel nozero overlap $Z_{Neel}(L)$for a chain of length L is given as

$$Z_{Neel} = 2^{\frac{L}{2}-1} + \frac{1}{2}B\Big(\frac{L}{2}, \frac{L}{4}\Big) + 1. \tag{A.1}$$

For simplicity here we restrict ourselves to the situation with L divisible by four. The strategy to prove (A.1) is to count all the possible parity-invariant BGT quantum numbers configurations. Let us consider the sector with fixed number of particles M, and a generic string content $\mathcal{S} = \{s_1, s_2, \ldots, s_M\}$. Here s_n is the number of n-strings, and one has the constraint $\sum_k k s_k = M$.
It is straightforward to check that total number of parity-invariant quantum number pairs $\mathcal{N}_n(L, \mathcal{S})$ in the n-string sector is given as

$$\mathcal{N}_n(L, \mathcal{S}) = \left\lfloor \frac{L}{2} - \frac{1}{2} \sum_{m=1}^{M} t_{nm} s_m \right\rfloor. \tag{A.2}$$

where $t_{nm} \equiv 2\mathrm{Min}(n, m) - \delta_{n,m}$. The number of parity-invariant quantum number configurations (i.e., eigenstates) $\mathcal{N}(L, \mathcal{S})$ compatible with string content $\mathcal{S}$ is obtained by choosing in all the possible ways the parity-invariant quantum number pairs independently in each n-string sector, which implies that

$$\mathcal{N}(L, \mathcal{S}) = \prod_{m=1}^{M} B\left(\mathcal{N}_m, \left\lfloor \frac{s_m}{2} \right\rfloor\right). \tag{A.3}$$

Here the product is because each string sector is treated independently, while the factor $1/2$ in $s_m/2$ is because since all quantum numbers are organized in pairs, only half of the quantum numbers have to be specified. Note that in each n-string sector only one zero momentum (i.e., zero quantum number) string is allowed, due to the Pauli principle. Moreover, s_m is odd (even) only if the zero momentum string is (not) present. The floor function $\lfloor \cdot \rfloor$ in (A.3) reflects that the quantum number of zero-momentum strings is fixed.
We now consider the string configurations with particle number $0 \leq \ell \leq M$ and fixed number of strings $1 \leq q \leq M/2$. Note that the maximul allowed string length is $M/2$ beacause of parity invariance. Note also that in determining q strings of different length are treated equally. Clearly, one has that $\sum_m s_m = q$. For a given fixed pair ℓ, q the total number of quantum number configurations is given as

$$\mathcal{N}'(L, \ell, q) = \sum_{\{\{s_m\} : \sum m s_m = \ell, \sum s_m = q\}} \mathcal{N}(L, \mathcal{S}), \tag{A.4}$$

where the sum is over the content $\{s_m\}_{m=1}^{M}$ compatible with the constraints $\sum_m s_m = q$ and $\sum_m m s_m = \ell$. The strategy is to write a recursive relation for $\mathcal{N}'(L, \ell, q)$. To this purpose it is useful to consider the shifted string content $\mathcal{S}'$ defined as

$$\mathcal{S}' \equiv \{s_{m+1}\} \quad \text{with } s_m \in \mathcal{S},\ \forall m. \tag{A.5}$$

Using the definition of t_{ij}, it is straightforward to derive that

$$t_{ij} = t_{i-1,j-1} + 2, \tag{A.6}$$

which implies that $\mathcal{N}_n(L, \mathcal{S})$ (see (A.2)) satisfies the recursive equation

$$\mathcal{N}_n(L, \mathcal{S}) = \mathcal{N}_{n-1}(L - 2q, \mathcal{S}'). \tag{A.7}$$

After substituting in (A.3) one obtains

$$\mathcal{N}(L,\mathcal{S}) = B\Big(\mathcal{N}_1(L,\mathcal{S}), \Big\lfloor \frac{s_1}{2} \Big\rfloor\Big)\mathcal{N}(L-2q,\mathcal{S}'). \tag{A.8}$$

Finally, after substituting (A.8) in (A.4), one obtains a recursive relation for $\mathcal{N}'(L,\ell,q)$ as

$$\mathcal{N}'(L,\ell,q) = \sum_{s=0}^{q-1} B\Big(\frac{L}{2}-q+\Big\lfloor\frac{s}{2}\Big\rfloor, \Big\lfloor\frac{s}{2}\Big\rfloor\Big)\mathcal{N}'\left(L-2q,\ell-q,q-s\right), \tag{A.9}$$

with the constraint that when $\ell = q$ one has

$$\mathcal{N}'(L,q,q) = B\Big(\Big\lfloor\frac{L-q}{2}\Big\rfloor, \Big\lfloor\frac{q}{2}\Big\rfloor\Big). \tag{A.10}$$

This is obtained by observing that if $\ell = q$ only 1-strings are allowed and (A.2) gives $\mathcal{N}_n(L,\mathcal{S}) = \lfloor (L-q)/2 \rfloor$.

It is straightforward to check that for even q the ansatz

$$\mathcal{N}'(L,\ell,q) = \frac{q}{\ell} B\Big(\frac{L-\ell}{2}, \frac{q}{2}\Big) B\Big(\frac{\ell}{2}, \frac{q}{2}\Big), \tag{A.11}$$

satisfies (A.9). For odd q the solution of (A.9) is

$$\mathcal{N}'(L,\ell,q) = \frac{\ell-q+1}{\ell} B\Big(\frac{L-\ell}{2}, \frac{q-1}{2}\Big) B\Big(\frac{\ell}{2}, \frac{q-1}{2}\Big). \tag{A.12}$$

The number of eigenstates in the sector with ℓ particles with nonzero Néel overlap $Z'_{Neel}(L,\ell)$ are obtained by summing over all possible values of q as

$$Z'_{Neel}(L,\ell) = \sum_{q=1}^{\ell} \mathcal{N}'(L,\ell,q). \tag{A.13}$$

It is convenient to split the summation in (A.13) considering odd values of q and even q separately. For odd q one obtains

$$\sum_{k=0}^{\ell/2-1} \mathcal{N}'(L,\ell,2k+1) = B\Big(\frac{L}{2}-1, \frac{\ell}{2}-1\Big), \tag{A.14}$$

while for even q one has

$$\sum_{k=0}^{\ell/2} \mathcal{N}'(L,\ell,2k) = B\Big(\frac{L}{2}-1, \frac{\ell}{2}\Big). \tag{A.15}$$

Putting everything together one obtains

$$Z'_{Neel}(L,\ell) = B\Big(\frac{L}{2}-1, \frac{\ell}{2}-1\Big) + B\Big(\frac{L}{2}-1, \frac{\ell}{2}\Big). \tag{A.16}$$

The total number of eigenstates with nonzero Néel overlap $Z_{Neel}(L)$ (cf. (A.1)) is obtained from (A.16) by summing over the allowed values of $\ell = 2k$ with $k = 0, 1, \ldots, \ell/2$.

Note that the total number Z_{MG} of parity-invariant eigenstates having non zero overlap with the Majumdar-Ghosh state is obtained from Eq (A.16) replacing $\ell = L/2$, to obtain

$$Z_{MG} = B\Big(\frac{L}{2}-1, \frac{L}{4}-1\Big) + B\Big(\frac{L}{2}-1, \frac{L}{4}\Big). \tag{A.17}$$

Physically, this is due to the fact that the Majumdar-Ghosh state is invariant under $SU(2)$ rotations, which implies that only eigenstates with zero total spin $S = 0$ can have non zero overlap.

Appendix B. Excluding the zero-momentum strings

Here we demonstrate that the total number of eigenstates with nonzero Néel overlap, which do not contain zero-momentum strings, $\widetilde{Z}_{Neel}(L)$ is given as

$$\widetilde{Z}_{Neel}(L) = B\Big(\frac{L}{2}, \frac{L}{4}\Big). \tag{B.1}$$

Given a generic M-particle eigenstate of the XXX chain, due to parity invariance, if one excludes the zero-momentum strings only n-strings with length $n \leq M/2$ are allowed. Similarly, the string content is of the form $\widetilde{\mathcal{S}} \equiv \{\tilde{s}_1, \ldots, \tilde{s}_{M/2}\}$, i.e., $\tilde{s}_m = 0\ \forall m > M/2$. Note that due to parity invariance and to the exclusion of the zero-momentum strings one has that $\tilde{s}_m$ is always an even integer. Clearly one has $\sum_{m=1}^{M/2} m\tilde{s}_m = M$.
The total number of parity-invariant quantum numbers $\widetilde{\mathcal{N}}_n$ in the n-string sector is given as

$$\widetilde{\mathcal{N}}_n(L, \widetilde{\mathcal{S}}) = \frac{L}{2} - \frac{1}{2}\sum_{m=1}^{M/2} t_{nm}\tilde{s}_m. \tag{B.2}$$

The proof now proceeds as in Appendix A. One can define the total number of eigenstates with nonzero Néel overla in the sector with ℓ particles and q different strings as $\widetilde{\mathcal{N}}'(L, \ell, q)$. Note that due to parity invariance and the exclusion of zero-momentum strings, q must be even. It is straigtforward to show that $\widetilde{\mathcal{N}}'(L, \ell, q)$ obeys the recursive relation

$$\widetilde{\mathcal{N}}'(L, \ell, q) = \sum_{s=0}^{q/2-1} B\Big(\frac{L}{2} - q + s, s\Big)\widetilde{\mathcal{N}}'\Big(L - 2q, \frac{\ell - q}{2}, \frac{q}{2} - s\Big), \tag{B.3}$$

with the constraint

$$\widetilde{\mathcal{N}}'(L, 1, 1) = \frac{L}{2} - 1. \tag{B.4}$$

It is straightforward to check that the solution of (B.3) is given as

$$\widetilde{\mathcal{N}}'(L, \ell, q) = \frac{L - 2\ell + 2}{L - \ell + 2} B\Big(\frac{L - \ell}{2} + 1, q\Big) B\Big(\frac{\ell}{2} - 1, \frac{q}{2} - 1\Big). \tag{B.5}$$

After summing over the allowed values of $q = 2k$ with $k = 1, 2, \ldots, \ell/2$ one obtains the total number of eigenstaets with nonzero Néel overlap at fixed number of particles ℓ $\widetilde{Z}'_{Neel}(L, \ell)$ as

$$\widetilde{Z}'_{Neel}(L, \ell) = B\Big(\frac{L}{2}, \frac{\ell}{2}\Big) - B\Big(\frac{L}{2}, \frac{\ell}{2} - 1\Big). \tag{B.6}$$

Summing over ℓ one obtains (**??**). Similar to (A.17) the total number of eigenstates $\widetilde{Z}_{MG}$ with no zero-momentum strings having non-zero overlap with the Majumdar-Ghosh state is obtained from (B.6) replacing $\ell \to L/2$, to obtain

$$\widetilde{Z}_{MG} = B\Big(\frac{L}{2}, \frac{L}{4}\Big) - B\Big(\frac{L}{2}, \frac{L}{4} - 1\Big). \tag{B.7}$$

Interestingly, using (A.17) and (B.7), one obtains that the ratio $\widetilde{Z}_{MG}/Z_{MG}$ is given as

$$\frac{\widetilde{Z}_{MG}}{Z_{MG}} = \frac{4}{4+L}. \tag{B.8}$$

Appendix C. Exact Néel and Majumdar-Ghosh overlaps for a small Heisenberg chain

In this section we provide exact diagonalization results for the overlap of both the Néel state and the Majumdar-Ghosh (MG) state with all the eigenstates of the Heisenberg spin chain with $L = 12$ sites. We also provide the corresponding results obtained using the string hypothesis and the overlap formulas (26) and (33), restricting ourselves to eigenstates with no zero-momentum strings.

Appendix C.1. Néel overlap

The overlaps between all the eigenstates of the Heisenberg spin chain and the Néel state are reported in Table C1. The first column in the Table shows the string content $\mathcal{S} \equiv \{s_1, \ldots, s_M\}$, with M being the number of finite rapidities. The number of infinite rapidities $N_\infty = L/2 - M$ is also reported. Note that eigenstates containing infinite rapidities correspond to different S_z eigenvalue. The second column shows $2I_n^+$, with I_n the Bethe-Gaudin-Takahashi quantum number identifying the BGT rapidity of the n-string. Due to the parity invariance only the positive quantum numbers are reported. The total number of independent strings, i.e., $q \equiv \sum_j s_j$, is reported in the third column. The fourth column is the eigenstate's energy eigenvalue E. The last two columns show the squared Néel overlaps and the corresponding result obtained using the Bethe-Gaudin-Takahashi equations, respectively. In the last column only the case with no zero-momentum strings is considered. The deviations from the exact diagonalization results (digits with different colors) have to be attributed to the string hypothesis. Notice that the overlap between the Néel state and the $S_z = 0$ eigenstate in the sector with maximal total spin $S = L/2$ (first column in Table C1), is given analytically as $2/B(L, L/2)$, with $B(x, y)$ the Newton binomial.

Figure C1 plots the squared overlaps $|\langle\lambda|N\rangle|^2$ between the Néel state and the eigenstates of the chain. The overlaps are plotted against the eigenstate energy density $E/L \in [-\log(2), 0]$. The circles are exact diagonalization results for all the chain eigenstates (382 eigenstates), whereas the crosses denote the overlaps calculated using formula (26), and the Bethe-Gaudin-Takahashi equations. Note that only the eigenstates with no zero-momentum strings are shown (252 eigenstates) in the Figure. Panel (a) in the Figure is an overview of all the results. Panels (b)-(d) correspond to zooming to the smaller overlap values $|\langle N|\lambda\rangle| \lesssim 0.02$, $|\langle N|\lambda\rangle| \lesssim 0.002$, and $|\langle N|\lambda\rangle| \lesssim 10^{-5}$.

Clearly, the overlaps decay rapidly upon increasing the energy density. This is expected since the XXX Hamiltonian expectation value over the Néel state is $\langle N|H|N\rangle = -1/2$. Importantly, the agreement between the exact diagonalization results and the results

obtained using the BGT equations (**??**) is excellent, confirming the validity of the string hypothesis.

Bethe states with nonzero Néel overlap ($L = 12$)

String content	$2I_n^+$	q	E	$\|\langle\lambda\|N\rangle\|^2$ (exact)	$\|\langle\lambda\|N\rangle\|^2$ (BGT)
6 inf	-	-	0	0.002164502165	0.002164502165
{2,0} 4 inf	1_1	2	−3.918985947229	0.096183409244	0.096183409244
	3_1		−3.309721467891	0.011288497947	0.011288497947
	5_1		−2.284629676547	0.004542580506	0.004542580506
	7_1		−1.169169973996	0.002752622983	0.002752622983
	9_1		−0.317492934338	0.002116006203	0.002116006203
{4,0,0,0} 2 inf	1_13_1	4	−7.070529325964	0.310133033838	0.310133033838
	1_15_1		−5.847128730477	0.129277023687	0.129277023687
	1_17_1		−4.570746557876	0.085992436024	0.085992436024
	3_15_1		−5.153853093221	0.015256395523	0.015256395523
	3_17_1		−3.916336243695	0.010091113504	0.010091113504
	5_17_1		−2.817696043731	0.004059780228	0.004059780228
{0,2,0,0} 2 inf	1_2	2	−1.905667167442	0.001207238321	0.00120724540 6
	3_2		−1.368837200825	0.002340453815	0.00232572471 3
	5_2		−0.681173793635	0.001921010489	0.00193900139 6
{1,0,1,0} 2 inf	0_10_3	2	−2.668031843135	0.034959609810	-
{6,0,0,0,0,0} 0 inf	$1_13_15_1$	6	−8.387390917445	0.153412152966	0.153412152966
{2,2,0,0,0,0} 0 inf	1_11_2	4	−5.401838225870	0.040162686361	0.04 1042488913
	3_11_2		−4.613929948329	0.004636541934	0.004 730512604
	5_11_2		−3.147465758841	0.001335522556	0.001337 334035
{3,0,1,0,0,0} 0 inf	$0_12_10_3$	4	−6.340207488736	0.052743525774	-
	$0_14_10_3$		−5.203653009936	0.015022005621	-
	$0_16_10_3$		−3.788693957250	0.011144489334	-
{1,0,0,0,1,0} 0 inf	0_10_5	2	−2.444293750583	0.005887902992	-
{0,0,2,0,0,0} 0 inf	1_3	2	−1.111855930538	0.001342476001	0.00 184980817
{0,1,0,1,0,0} 0 inf	0_20_4	2	−1.560671012472	0.000026982174	-

Table C1. All Bethe states for $L = 12$ having nonzero overlap with the zero-momentum Néel state. The first column shows the string content of the Bethe states, including the number of infinite rapidities. The second and third column show $2I_n^+$, with I_n^+ the BGT quantum numbers identifying the different states, and the number q of independent strings. In the second column only the positive BGT numbers are shown. The fourth column is the Bethe state eigenenergy. Finally, the last two columns show the exact overlap with the Néel state and the approximate result obatained using the BGT equations. In the last column Bethe states containing zero-momentum strings are excluded. Deviations from the exact result (digits with different colors) are attributed to the string hypothesis.

Appendix C.2. Majumdar-Ghosh overlap

The overlap between the Heisenberg chain eigenstates with the Majumdar-Ghosh state are shown in Table C2. The conventions on the representation of the eigenstates is the same as in Table C1. Note that in contrast with the Néel state, only the eigenstates with zero total spin $S = 0$ have non zero overlap, i.e., no eigenstates with infinite rapidities are present, which reflect that the Majumdar-Ghosh state is unvariant under $SU(2)$ rotations.

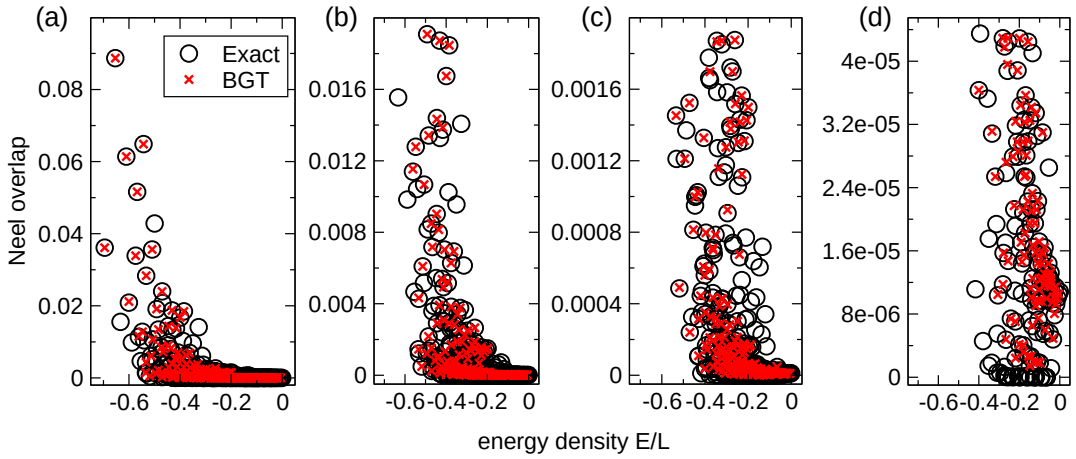

Figure C1. The squared overlap $|\langle N|\lambda\rangle|^2$ between the the Neel state $|N\rangle$ and the eigenstates $|\lambda\rangle$ of the XXX chain with $L = 20$ sites. Only non-zero overlaps are shown. In all the panels the x-axis shows the eigenstate energy density E/L. The circles are the exact diagonalization results for all the non-zero overlaps. The crosses are the Bethe ansatz results obtained using the Bethe-Gaudin-Takahashi equations. The missing crosses correspond to eigenstates containing zero-momentum strings. (a) Overview of all the non-zero overlaps. (b)(c)(d) The same overlaps as in (a) zooming in the regions $[0, 0.2]$, $[0, 0.020]$, and $[0, 4 \cdot 10^{-5}]$. The discrepancies between the ED and the Bethe ansatz results are attributed to the string deviations.

Bethe states with nonzero Néel overlap ($L = 12$)

String content	$2I_n^+$	q	E	$\lvert\langle\lambda\rvert MG\rangle\rvert^2$ (exact)	$\lvert\langle\lambda\rvert MG\rangle\rvert^2$ (BGT)
{6,0,0,0,0,0}	$1_1 3_1 5_1$	6	−8.387390917445	0.716615769224	0.716615769224
{2,2,0,0,0,0}	$1_1 1_2$	4	−5.401838225870	0.055624700196	0.054033366543
	$3_1 1_2$		−4.613929948329	0.005687428810	0.005582983043
	$5_1 1_2$		−3.147465758841	0.002107475934	0.002107086933
{3,0,1,0,0,0}	$0_1 2_1 0_3$	4	−6.340207488736	0.205891158647	-
	$0_1 4_1 0_3$		−5.203653009936	0.038832154450	-
	$0_1 6_1 0_3$		−3.788693957250	0.006019410923	-
{1,0,0,0,1,0}	$0_1 0_5$	2	−2.444293750583	0.000129601311	-
{0,0,2,0,0,0}	1_3	2	−1.111855930538	0.000011727787	0.000012785580
{0,1,0,1,0,0}	$0_2 0_4$	2	−1.560671012472	0.000330572718	-

Table C2. All Bethe states for $L = 12$ having nonzero overlap with the zero-momentum Majumdar-Ghosh (MG) state. The first column shows the string content of the Bethe states. The second and third column show $2I_n^+$, with I_n^+ the BGT quantum numbers identifying the different states, and the number q of independent strings. In the second column only the positive BGT numbers are shown. Note that, in contrast to Table C1 no states with infinite rapidities are present. The fourth column is the Bethe state eigenenergy. Finally, the last two columns show the exact overlap with the MG state and the approximate result obatained using the BGT equations. In the last column Bethe states containing zero-momentum strings are excluded. Deviations from the exact result (digits with different colors) are attributed to the string hypothesis.

[1] I. Bloch, J. Dalibard, and W. Zwerger, Rev. Mod. Phys. **80**, 885 (2008).
[2] M. Greiner, O. Mandel, T. Hänsch, and I. Bloch, Nature (London) **419**, 51 (2002).

[3] T. Kinoshita, T. Wenger, and D. S. Weiss, Nature (London) **440**, 900 (2008).
[4] S. Hofferberth, I. Lesanovsky, B. Fischer, T. Schumm, and J. Schiedmayer, Nature (London) **449**, 324 (2007).
[5] S. Trotzky, Y.-A. Chen, A. Flesch, I. P. McCulloch, U. Schollwöck, J. Eisert, and I. Bloch, Nature Phys. **8**, 325 (2012).
[6] M. Gring, M. Kuhnert, T. Langen, T. Kitagawa, B. Rauer, M. Schreitl, I. Mazets, D. A. Smith, E. Demler, and J. Schmiedmayer, Science **337**, 6100 (2012).
[7] M. Cheneau, P. Barmettler, D. Poletti, M. Endres, P. Schaua, T. Fukuhara, C. Gross, I. Bloch, C. Kollath, and S. Kuhr, Nature (London) **481**, 484 (2012).
[8] U. Schneider, L. Hackeruller, J. P. Ronzheimer, S. Will, S. Braun, T. Best, I. Bloch, E. Demler, S. Mandt, D. Rasch, and A. Rosch, Nature Phys. **8**, 213 (2012).
[9] M. Kuhnert, R. Geiger, T. Langen, M. Gring, B. Rauer, T. Kitagawa, E. Demler, D. Adu Smith, and J. Schmiedmayer, Phys. Rev. Lett. **110**, 090405 (2013).
[10] T. Langen, R. Geiger, M. Kuhnert, B. Rauer, and J. Schmiedmayer, Nature Phys. **9**, 640 (2013).
[11] F. Meinert, M. J. Mark, E. Kirilov, K. Lauber, P. Weinmann, A. J. Daley, and H.-C. Nagerl, Phys. Rev. Lett. **111**, 053003 (2013).
[12] T. Fukuhara, A. Kantian, M. Endres, M. Cheneau, P. Schaua, S. Hild, C. Gross, U. Schollwöck, T. Giamarchi, I. Bloch, and S. Kuhr, Nature Phys. **9**, 235 (2013).
[13] J. P. Ronzheimer, M. Schreiber, S. Braun, S. S. Hodgman, S. Langer, I. P. McCulloch, F. Heidrich-Meisner, I. Bloch, and U. Schneider, Phys. Rev. Lett. **110**, 205301 (2013).
[14] S. Braun, M. Friesdorf, S. Hodgman, M. Schreiber, J. Ronzheimer, A. Riera, M. del Rey, I. Bloch, J. Eisert, and U. Schneider, PNAS **112**, 3641 (2015).
[15] T. Langen, S. Erne, R. Geiger, B. Rauer, T. Schweigler, M. Kuhnert, W. Rohringer, I. E. Mazets, T. Gasenzer, J. Schmiedmayer, Science **348**, 6231 (2015).
[16] A. Polkovnikov, K. Sengupta, A Silva, and M. Vengalattore, Rev. Mod. Phys. **83**, 863 (2011).
[17] M. Takahashi, *Thermodynamics of one-dimensional solvable models*, Cambridge University Press, Cambridge, 1999.
[18] S.-J. Gu, N. M. R. Peres, Y.-Q. Li, Eur. Phys. J. B **48**, 157 (2005).
[19] M. P. Grabowski and P. Mathieu, Ann. Phys. N.Y. **243**, 299 (1995).
[20] H. Bethe, Z. Phys. **71**, 205 (1931).
[21] J. Mossel and J.-S. Caux, J. Phys. A: Math. Theor. **45**, 255001 (2012).
[22] B. Pozsgay, J. Stat. Mech. (2013) P07003.
[23] V. E. Korepin, N. M. Bogoliubov, and A. G. Izergin, *Quantum Inverse Scattering Methods and Correlation Functions*, Cambridge University Press, Cambridge, 1997.
[24] D. P. Landau and K. Binder, *A Guide to Monte Carlo Simulations in Statistical Physics*, Cambridge University Press, Cambridge, 2000.
[25] L. D. Faddeev, arXiv:9605187.
[26] C. N. Yang and C. P. Yang, J. Math. Phys. **10**, 1115 (1969).
[27] P. Calabrese and P. Le Doussal, J. Stat. Mech. (2014) P05004.
[28] V. Alba, arXiv:1507.06994.
[29] H. Bethe, Zur Theorie der Metalle. I. Eigenwerte und Eigenfunktionen der linearen Atomkette, Z. Phys. **71**, 205 (1931).
[30] M. Brockmann, J. De Nardis, B. Wouters, and J.-S. Caux, J. Phys. A: Math. Theor. **47**, 345003 (2014).
[31] M. Brockmann, J. De Nardis, B. Wouters, and J.-S. Caux, J. Phys. A: Math. Theor. **47**, 145003 (2014).
[32] M. Brockmann, J. Stat. Mech. (2014) P05006.
[33] B. Pozsgay, J. Stat. Mech. (2014) P06011.
[34] P. Calabrese and J.-S. Caux, Phys. Rev. Lett. **98**, 150403 (2007).
[35] P. Calabrese and J.-S. Caux, J. Stat. Mech. P08032 (2007).
[36] J. De Nardis, B. Wouters, M. Brockmann, and J.-S. Caux, Phys. Rev. A **89**, 033601 (2014).

[37] B. Pozsgay, M. Mestyán, M. A. Werner, M. Kormos, G. Zaránd, and G. Takács, Phys. Rev. Lett. **113**, 117203 (2014).
[38] B. Wouters, M. Brockmann, J. De Nardis, D. Fioretto, M. Rigol, and J.-S. Caux, Phys. Rev. Lett. **113**, 117202 (2014).
[39] M Mestyán, B. Pozsgay, G. Takács, and M. A. Werner, J. Stat. Mech. (2015) P04001.
[40] E. Ilieveski, J. De Nardis, B. Wouters, J.-S. Caux, F. H. Essler, and T. Prosen, arXiv:1507.02993.
[41] M. Brockmann, B. Wouters, D. Fioretto, J. De Nardis, R. Vlijm, and J.-S. Caux, J. Stat. Mech. (2014) P12009.
[42] P. P. Mazza, J.-M. Stéphan, E. Canovi, V. Alba, M. Brockmann, and M. Haque, arXiv:1509.04666.
[43] M. Fagotti and F. H. Essler, J. Stat. Mech. (2013) P07012.
[44] M. P. Grabowski and P. Mathieu, Ann. Phys. N.Y. **243**, 299 (1995).
[45] M. H. Quenouille, Ann. Math. Statist. **20**, 355 (1949).
[46] U. Wolff, Comput. Phys. Comm. **156**, 143 (2004).
[47] L. Piroli and P. Calabrese, J. Phys. A **47**, 385003 (2014).